Journal of Forestry Research (2026) 37:79
https://doi.org/10.1007/s11676-026-02016-z

ORIGINAL PAPER

Forests in a semi-arid climate die with a memory: satellite signals predict forest mortality years after drought

Filippos Eliades[1,2] · Dimitrios Sarris[3,4] · Felix Bachofer[5] · Silas Michaelides[2] · Chris Danezis[1,2] · Diofantos Hadjimitsis[1,2]

Received: 10 September 2025 / Accepted: 8 January 2026

Abstract Widespread tree mortality is increasingly associated with extreme drought, yet its mechanisms remain poorly understood. To address this, we investigated which indicators most accurately delineate the relationship between climatic stressors and satellite-derived metrics related to tree crown/forest canopy conditions and forest decline for conifers and evergreen broadleaves. The study was performed between 1990 and 2020 in woodlands of Cyprus dominated by *Juniperus phoenicea*, *Pinus brutia*, and *Quercus alnifolia* (endemic to Cyprus). Landsat 5, 7, 8 and 9 images were used to assess the condition of tree crowns via 8 remote sensing (RS) indicators (NDMI, EVI, GPP, LAI, NBR, NDVI, NDWI, SAVI) correlated, thereafter, with the SPI, SPEI and PDSI drought indicators. Our findings clearly outline that very severe drought conditions <−2 for the SPI-12 and the SPEI-12, or <−5 for the PDSI-12, exceeded the capacity of all 3 species to sustain healthy stands at habitats representing the xeric limits of their natural distribution range in Europe. Very low precipitation appears as the driving force. However, starting from the year of drought induced mortality and including the years that followed, their annual vegetation's response via decadal monitoring was related to climate averaged over 4 to 7 past years (including the year of monitoring) depending on species. Observed multi-year associations are consistent with a 'memory' effect that may reflect cumulative depletion and slow recharge of deeper, root-accessible moisture pools; however, our remote-sensing indicators do not directly perceive subsurface storage. NBR and NDMI were significantly connected with climatic variability, as described by the SPI or SPEI for the *J. phoenicea* and by the PDSI for the *P. brutia*, before and at the first years after mortality has occurred. After some years after the mortality year, the decadal response of vegetation to climate was better described by the NDVI. Before oak mortality the RS indicators applied failed to capture the evergreen vegetation dynamic of *Q. alnifolia* dense stands. Thereafter, the NDVI provides the highest accuracy, as the oaks likely experienced more severe and faster defoliation than the conifers, reducing their vegetation density at levels detectable by the NDVI. Thus, our study highlights the importance of considering long-term drivers for tree foliage-defoliation status, dependent on species type and habitat-specific water availability. This understanding can explain the types of droughts (seasonal to multiyear) that can trigger tree mortality under climate change.

Project funding: This research was funded by the 'EXCELSIOR' project (European Union's Horizon 2020 Research and Innovation Programme) (Grant No.: 857510).

The online version is available at https://link.springer.com/

Corresponding editor: Lei Yu.

Supplementary Information The online version contains supplementary material available at https://doi.org/10.1007/s11676-026-02016-z.

✉ Filippos Eliades
fa.eliades@edu.cut.ac.cy

[1] Remote Sensing and GeoEnvironment Lab, Department of Civil Engineering and Geomatics, Cyprus University of Technology, Limassol, Cyprus

[2] Eratosthenes Centre of Excellence, Limassol, Cyprus

[3] KES Research Centre, Nicosia, Cyprus

[4] KES College, Nicosia, Cyprus

[5] German Aerospace Center (DLR), Earth Observation Center (EOC), Wessling, Germany

Published online: 03 March 2026

Keywords Tree mortality · Forest decline · Climate change · Remote sensing · Drought

Abbreviations

ET	Evapotranspiration
EVI	Enhanced Vegetation Index
fAPAR	Fraction of Absorbed Photosynthetically Active Radiation
GHCN	Global Historical Climatology Network
GPP	Gross primary production
LAI	Leaf Area Index
LUE	Light use efficiency
NBR	Normalized burn ratio
NDMI	Normalized Difference Moisture Index
NDVI	Normalized Difference Vegetation Index
NDWI	Normalized Difference Water Index
NOAA	National Oceanic and Atmospheric Administration
PAR	Photosynthetically active radiation
PDSI	Palmer Drought Severity Index
PET	Potential evapotranspiration
P-PET	Precipitation minus potential evapotranspiration
SAVI	Soil Adjusted Vegetation Index
SPEI	Standardized Precipitation–Evapotranspiration Index
SPI	Standardized Precipitation Index
VI	Vegetation Index

Introduction

In recent decades, numerous episodes of forest decline and drought-driven tree mortality have been documented (Hartmann et al. 2022; Eliades et al. 2024). These mortality events pose a critical challenge for forests and the ecosystem services they provide, especially under future climate scenarios that project substantial warming and widespread drying across mid-latitude regions (Seager et al. 2007; Choat et al. 2012; Cook et al. 2014; McMahon et al. 2019). Tree mortality has already been on the rise across extensive regions with Mediterranean climate (Allen et al. 2010; Eliades et al. 2024), primarily driven by the combined effects of climate warming and precipitation decline leading to drought, followed by other biotic factors. While the mechanisms governing these processes are complex, current evidence suggests that hydraulic failure, where water transport within the tree is critically disrupted, is the primary driver of drought-induced tree mortality (Choat et al. 2012).

These drying trends are likely to amplify tree mortality rates and contribute to extensive forest tree mortality events, particularly at rear-edge distribution ranges of tree species (Sarris et al. 2011; Dorman et al. 2015a; Mazza et al. 2021; Sarris and Christodoulakis 2024). Moreover, the impacts of droughts on forests can vary substantially, even under similar levels of drought severity, due to differences in species composition, site conditions, and ecosystem traits (Vetter et al. 2008; Shukla et al. 2015). Gaining a deeper understanding of the climatic factors influencing tree mortality across extensive spatial scales can assist in designing the strategies that enable proactive management to address potential tree mortality events (Mazza et al. 2018). To achieve this, implementing a reliable framework to evaluate forest health is critical. Such approach can integrate meteorological data with data from remote sensing of vegetation in the effort to examine the relationships between rising temperatures, water deficits, forest decline and tree mortality. For instance, the Normalized Difference Vegetation Index (NDVI) has been widely applied as a proxy for photosynthetic activity and has been shown to be closely linked to biodiversity (Dubinin et al. 2018).

Variability in climate leading to extreme events and disturbances can disrupt ecosystem productivity (Carpenter and Turner 2000), with the impact lasting from a few hours to several years (Thom et al. 2013). While long-term climate change occurs gradually over decades to centuries, short-term climate variability—such as extreme weather events and seasonal anomalies—can act as rapid disturbances that abruptly impact ecosystems, e.g., windthrow and frost. Tree mortality is also affected by slow-changing variables that evolve gradually over time. These include environmental attributes, such as gradual depletion of deeper moisture "pools" (Sarris et al. 2007, 2013; Sarris and Mazza 2021b). While harsh environments found at the limits of tree species distribution are associated with elevated mortality rates, favorable conditions can also increase the risk of individual tree loss. Enhanced growth in such conditions can lead to increased competition for resources, such as light, and greater vulnerability to natural events, like windthrow (Buma and Wessman 2011; Stephenson et al. 2011).

Integrating both rapid and gradual factors presents an ongoing challenge in the study of tree mortality across broad spatial scales. Comprehensive annual datasets on tree mortality are essential for linking mortality to short-term variables, such as intra- and inter-annual climate variability. However, such datasets are typically restricted to well-monitored, long-term research sites (Van Mantgem et al. 2009) which limits their applicability in deriving consistent large-scale patterns. In contrast, forest inventory data can offer insights into mortality across extensive regions (Hember et al. 2017). Yet, due to their extended intervals, often spanning five to ten years, their practical usefulness in revealing mortality responses to climate dynamics and extreme weather events is constrained. Such data gaps have so far hindered the development of a comprehensive understanding of tree mortality patterns on larger spatial scales (Tomppo et al. 2010). The

combined use of remote sensing tools and meteorological data can address these challenges.

This study aims to investigate the relationship between remotely sensed indicators of forest decline and meteorological drought indicators across seasonal, monthly, and multi-year timescales. On the one hand, we examine commonly used satellite-derived metrics reflecting canopy condition. On the other hand, we assess how these relate to standardized drought indicators in Mediterranean conifer and evergreen broadleaf forests, particularly at the ecological margins of their distribution. Understanding how different indicators respond to climate change across various regions and tree species will provide a more precise assessment of forest vulnerability. Addressing this knowledge gap can contribute to the development of early warning systems, thus enabling proactive measures to mitigate the effects of climate change on forests (Dakos et al. 2008).

To accomplish this objective, we conducted for the first time a comprehensive comparative analysis of eight remotely sensed indicators. These indicators, namely, Enhanced Vegetation Index (EVI), Gross Primary Productivity (GPP), Leaf Area Index (LAI), NBR, NDMI, NDVI, NDWI, and Soil-Adjusted Vegetation Index (SAVI), were selected based on their widespread use in global tree mortality assessments (Eliades et al. 2024) and are related to the state of forest vegetation/environment. We compared these remotely sensed indicators with three meteorological drought indicators (SPI, SPEI, and PDSI) to evaluate their relationship, before and after two major tree mortality events—one in 2008 across Cyprus, and another in 2016, especially affecting the Akamas region. The analysis was conducted on two conifers (*Juniperus phoenicea* L., *Pinus brutia* Ten.) and an evergreen broadleaf (the endemic *Quercus alnifolia* Poech) across three forest sites. All tree populations were at the southern-most (rear-edge) distribution ranges of the above species in the Mediterranean. To analyze tree response under varying climate dryness, a running correlation analysis was performed using moving analysis "windows" of 10 years to examine the relationship between tree crowns/foliage conditions and drought indicators (Sarris et al. 2007; Sarris and Christodoulakis 2024).

This study examines how climate influences the health of important Mediterranean forest species at the limits of their distribution range and whether remote sensing can effectively capture this effect to improve our understanding of tree mortality drivers. Specifically, we aim to: (a) investigate the relationship between the 2008 and 2016 forest mortality events in Cyprus and drought conditions; (b) identify the most effective drought and remote sensing vegetation indicators for explaining forest decline and mortality in conifers and evergreen broadleaves; and (c) determine the temporal scales at which these indicators are most effective. Addressing these questions may lead to the selection of the best performing indicators that can be adopted as early warning signals for tree mortality and as tools for mapping high-risk areas.

Materials and methods

A structured workflow for remote sensing-based drought assessment

For the needs of this study, we developed a structured, remote sensing-based workflow to assess drought impacts on forest ecosystems by integrating satellite-derived vegetation indicators with climatic drought indicators. Vegetation metrics were extracted from Landsat 5–9 Surface Reflectance products via Google Earth Engine (GEE), following standard pre-processing steps, including atmospheric correction, cloud and shadow masking, and radiometric scaling. Within each forest site, plots were delineated to generate time series for eight widely used drought-responsive indicators—EVI, GPP, LAI, NDVI, NDMI, NDWI, NBR, and SAVI—capturing structural, physiological, and moisture-related canopy conditions. Daily temperature and precipitation records from 1990 to 2020 were used to compute three meteorological drought indicators: the SPI, the SPEI, and the PDSI, ensuring temporal alignment with satellite observations. Data were analyzed at monthly, seasonal, annual, and multi-year scales, including 2–10 year running means to capture short- and long-term drought signals. To evaluate vegetation responses to climatic stress, statistical techniques such as Cook's Distance, Kalman filtering, and Spearman's correlation were applied, as shown in Fig. 1. The above remote sensing indicators (reflecting the structural, physiological, and moisture-related state of tree crowns and the forest canopy) were subsequently tested to assess the short and long-term sensitivity of tree foliage to precipitation (SPI) and drought (PDSI, and SPEI) variability, before and after the tree mortality events of 2008 and 2016. Our remote sensing indicators reflect canopy condition that integrates plant water status; any link to the root-accessible zone is inferred, not directly measured.

This approach was applied to three Mediterranean forest ecosystems in Cyprus—two coniferous (*J. phoenicea* and *P. brutia*) and one evergreen broadleaf (*Q. alnifolia*)—across the sites of Akamas, Machairas, and Stavrovouni. Akamas experienced extensive tree mortality during both the 2007–2008 mega-drought and a second event in 2016 (see Supplementary Table S1; Figs. 2, 3), while Machairas and Stavrovouni were affected primarily during the 2007–2008 event (see Supplementary Table S1; Figs. 2, 4, 5). The populations of the tree species under investigation were all close to the limits of their distribution range in the Mediterranean, and from habitats with limited moisture

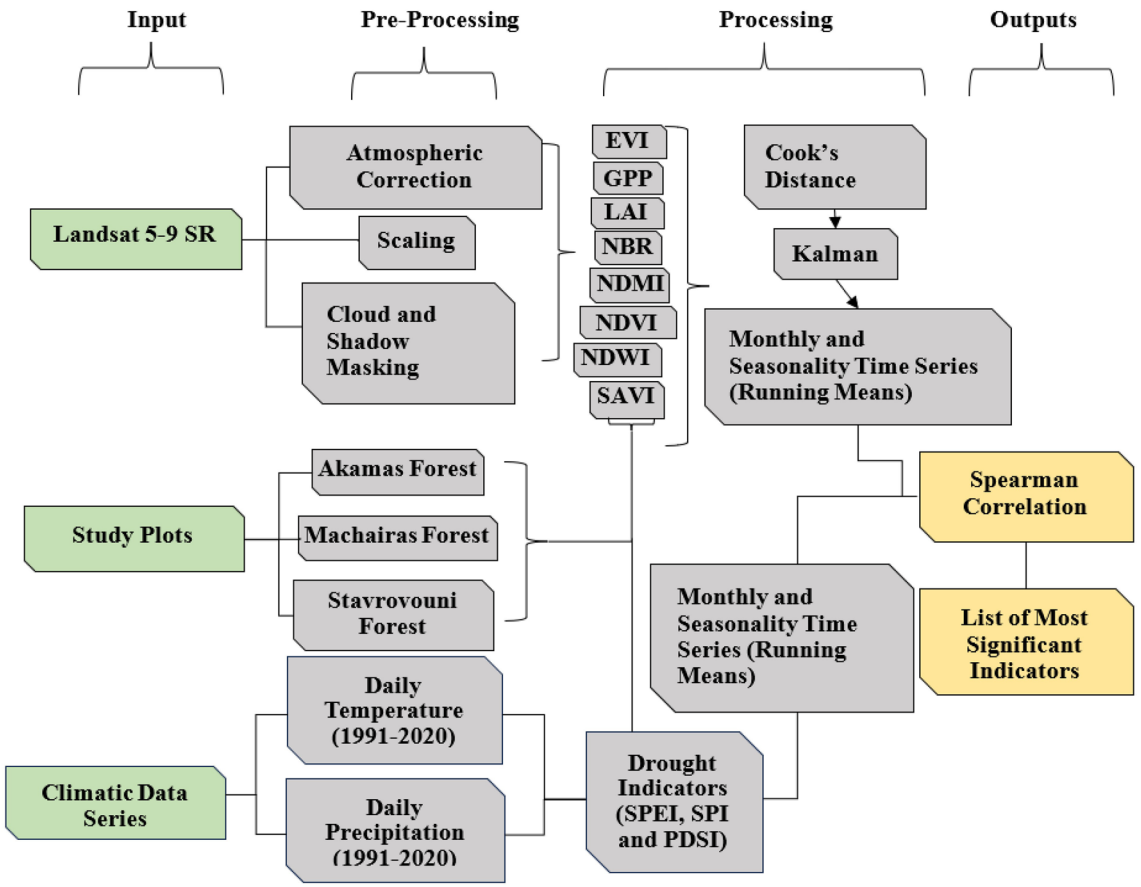

Fig. 1 Summary of the methodological workflow for assessing drought impacts on forest ecosystems

Fig. 2 The morphological map of Cyprus, with selected specific tree populations (encircled) within each study area: **a** Akamas, **b** Machairas, and **c** Stavrovouni

Fig. 3 Part of the study area in Akamas forest, with *J. phoenicea* mortality (encircled) in 2016 (2 km north–west of the 2008 mortality areas in the area) (Eliades 2016)

Fig. 4 Part of the study area in Machairas forest, with *Q. alnifolia* mortality (encircled) in 2008 (Eliades 2008)

availability due to topography (Sarris and Christodoulakis 2024) (Figs. 3, 4, 5).

Selected habitats and tree species populations

Annual precipitation in Cyprus ranges from about 300 mm in the central plains and eastern lowlands to 1100 mm at the peak of the Troodos massif (Meteorological Service 1986). Rainfall gradually diminishes on the more sheltered northern and eastern slopes of the island (Pashiardis and Michaelides 2009). The study area encompassed the regions of Akamas (35°02′51.7″N, 32°19′04.5″E), Machairas (34°55′29.3″N, 33°11′32.9″E), and Stavrovouni (34°54′08.3″N, 33°25′22.8″E) in Cyprus, as depicted in Fig. 2. These areas are covered with woodlands growing on rocky soils and are renowned for their unique biodiversity and ecological significance. The vegetation consists of coniferous forests dominated by *P. brutia* in Stavrovouni

Fig. 5 Part of the study area in Stavrovouni forest, with *P. brutia* mortality (encircled) in 2008 (Forest Department of Cyprus 2008)

and evergreen broadleaf *Q. alnifolia* in Machairas, both of which experienced substantial tree mortality in 2008, and of *J. phoenicea* in Akamas, where significant mortality was observed later, in 2016. These species populations were located at the rear-edge of their distribution ranges in the Mediterranean and in marginal habitats where drought stress impacts are most severe.

The selected *J. phoenicea* populations in the Akamas Peninsula cover an area of 10,805 m^2 at a relatively low elevation of 280 m above sea level, on south- and south-east-facing slopes with an incline of 15%–20%. The area receives an annual precipitation of approximately 450 mm. The underlain rocky geology with limited clay soils results in low water retention capacity, intensifying drought stress, as illustrated in Fig. 3.

Selected *Q. alnifolia* populations in Machairas (area = 19,179 m^2), grow at an elevation of 1220 m, and on northeast and east aspects, with an incline of steep slopes about 25%–30% and normal precipitation at approximately 700 mm per year. The rocky soil and steep slopes lead to rapid water runoff that further limit soil moisture availability, as depicted in Fig. 4.

Lastly, the *P. brutia* populations in the Stavrovouni forest (area = 75,055 m^2), grew at an elevation of 300 m, on northeast and east-facing slopes with an incline of 13%–16% receiving around 400 mm annually under normal climatological conditions. The underlying rocky substrates restrict water infiltration and retention, as shown in Fig. 5.

Satellite data

Satellite imagery from Landsat (MSS, TM, and ETM+ sensors, with spatial resolutions between 15 and 30 m), covering the period from 1990 to 2020 was retrieved through the Google Earth Engine; focusing on areas where tree mortality was clearly visible in the satellite imagery. The NDVI is among the most widely utilized indicators for monitoring vegetation in ecosystem studies (Eliades et al. 2024). NDVI represents a measure of vegetation productivity, relying on the assessment of radiation absorbed for photosynthesis (Sellers et al. 1992). It is also applied to determine parameters like Leaf Area Index, plant biomass, and moisture levels (Aguilar et al. 2012). The equation for NDVI is given by:

$$\mathrm{NDVI} = (\mathrm{NIR} - \mathrm{RED})/(\mathrm{NIR} + \mathrm{RED}) \quad (1)$$

where, NIR is the near-infrared reflectance (~0.83 µm), sensitive to the cell structure of leaves, and RED is the red reflectance (~0.65 µm) (Rouse 1974).

The EVI was designed to enhance the detection of vegetation signals by increasing sensitivity in areas with high biomass, improving vegetation monitoring by minimizing the influence of the canopy background signal, and reducing atmospheric effects (USGS 2025):

$$\mathrm{EVI} = (2.5(\mathrm{NIR} - \mathrm{RED}))/(\mathrm{NIR} + 6\,\mathrm{RED} - 7.5\mathrm{BLUE} + 1) \quad (2)$$

where, BLUE is the blue reflectance (~0.452–0.512 µm), used for atmospheric correction to minimize the effects of aerosol scattering and soil background noise.

Unlike NDVI, NDWI exhibits lower sensitivity to atmospheric scattering effects. The NDWI quantifies the presence of liquid water molecules in vegetation canopies that interact with incoming solar radiation and is calculated as (Gao 1996):

$$NDWI = (GREEN - NIR)/(GREEN + NIR) \quad (3)$$

where, GREEN is the green reflectance (~0.56 µm), which enhances the presence of water by maximizing its reflectance from water bodies.

The Leaf Area Index (LAI), defined as the total leaf surface area per unit of ground area ($m^2\ m^{-2}$), serves as an aggregate metric for characterizing the foliar component of vegetation canopy structure. LAI exhibits a simple linear relationship with EVI, which enhances vegetation monitoring by reducing atmospheric and soil background effects:

$$LAI = 0.3618 \times EVI - 0.11 \quad (4)$$

where, the values 0.3618 and −0.11 are constants derived from empirical research and calibration studies (Boegh et al. 2002).

SAVI is applied to adjust the NDVI for the impact of soil brightness, particularly in areas with sparse vegetative cover and is calculated as (Huete 1988):

$$SAVI = ((1 + L)(NIR - RED)) \div (NIR + RED + L) \quad (5)$$

where, L represents a canopy background adjustment factor. An L value of 0.5 in reflectance space has been shown to reduce soil brightness variations effectively and remove the need for extra calibration across different soil types.

The absolute value of the NDMI allows for the immediate identification of farm or field areas experiencing water stress, and it is calculated as (Gao 1996):

$$NDMI = (NIR - SWIR1) \div (NIR + SWIR1) \quad (6)$$

where, SWIR1 is the shortwave infrared reflectance (~1.64 µm), which is strongly influenced by the moisture content in vegetation and soil. NDMI is commonly used to assess vegetation water content and monitor drought conditions.

The trends in the NBR show a direct relationship with factors such as yearly precipitation, average climatic temperature and depth of soil, and it is calculated as (Keeley 2009):

$$NBR = (NIR - SWIR2) \div (NIR + SWIR2) \quad (7)$$

GPP refers to the total rate at which carbon is fixed by vegetation through photosynthesis. Therefore, both Light Use Efficiency (LUE) and the fraction of Absorbed Photosynthetically Active Radiation (fAPAR) are derived from Vegetation Indicators (VIs); GPP is calculated as the product of VIs and PAR. EVI, as a component of GPP, had the highest determination coefficient (R^2) among all VIs calculated from the relationship (Wu et al. 2010):

$$GPP = PAR \times EVI \times EVI \quad (8)$$

where, PAR in the Eastern Mediterranean basin is estimated as having an annual mean value of 0.454 (Jacovides et al. 2003).

Meteorological drought parameters

Daily temperature and precipitation data from three meteorological stations of the Cyprus Department of Meteorology—Akamas (Smiges; 35.0240°N, 32.3331°E; 273 m above sea level), Machairas (Kionia; 34.9202°N, 33.1976°E; 1,352 m above sea level), and Stavrovouni (Kornos; 34.8869°N, 33.4367°E; 341 m above sea level)—were used to calculate three drought indicators: SPI, SPEI, and PDSI. The dataset used spans from 1990 to 2020, providing a 30-year record essential for a robust drought assessment that included the documented tree mortality event of 2008 across Cyprus and 2016 in Akamas. To ensure the accuracy and reliability of data from the Akamas (Smiges) station, additional precipitation and temperature data were obtained from the nearby station in Polis Chrysochous, sourced from NOAA's Global Historical Climatology Network (GHCN), which provides long-term, ground-based climate observations worldwide. Additionally, ERA5 climate reanalysis data, produced by the European Centre for Medium-Range Weather Forecasts (ECMWF), were used for cross-validation of the station-based temperature and precipitation records. ERA5 offers high-resolution (0.25° grid) hourly climate data by assimilating ground-based observations, satellite measurements, and data from numerical weather prediction models, making it particularly useful for filling observational gaps in areas with limited ground station coverage (Hersbach et al. 2020; National Centers for Environmental Information (NCEI) 2025). Each station was selected for its geographic relevance and data quality, ensuring high-resolution and continuous daily observations. The long-term dataset facilitated a comprehensive analysis of temporal and spatial variations in precipitation and temperature anomalies, enabling the evaluation of both short- and long-term drought patterns in the region.

We adopted 12-month drought indices (SPI-12, SPEI-12, PDSI-12) to ensure direct comparability with the annually aggregated remote sensing vegetation indicators and to capture prolonged, cumulative moisture deficits that most strongly affect tree condition. We also computed shorter (3–6 months) and longer (24 months) windows; however, we prioritized 12 months to present a general, annual picture and to maintain year-to-year correlations (avoiding month-to-year mismatches). Patterns were broadly consistent across scales, but the 12-month aggregation provided the clearest

and most stable signal around the mortality (2008, 2016) and recovery intervals.

SPEI, which incorporates both precipitation (P) and potential evapotranspiration (PET), was used to assess drought conditions. Unlike SPI which relies solely on precipitation anomalies (Vicente-Serrano et al. 2010), SPEI accounts for temperature-driven changes in water demand, making it more reflective of hydrological anomalies caused by temperature variability. This distinction is critical, as evapotranspiration influences soil moisture and vegetation water content (National Centers for Environmental Information (NCEI) 2025). SPEI calculations require mean temperature, latitude and continuous monthly data spanning at least 30 years.

SPEI values are computed over specific time scales (e.g., 1, 3, 6, 12, and 24 months), reflecting the cumulative P-PET (Precipitation–Potential Evapotranspiration) anomalies for the selected period compared to the long-term historical record. For instance, the 3-month SPEI (SPEI-3) for March is calculated using the cumulative P-PET for January, February, and March, compared with the historical record for the same period. Shorter time scales, such as SPEI-1, capture short-duration droughts (e.g., soil moisture deficits), while longer time scales, such as SPEI-12, SPEI-24 or even longer, represent prolonged droughts affecting reservoirs and groundwater availability.

The PDSI, a composite drought indicator, was also employed to capture both current-month and lagged effects of precipitation and temperature on drought conditions (Alley 1984). Negative PDSI values indicate drought, while positive values reflect wetter-than-average conditions. Together, these meteorological drought indicators provided a robust framework for analyzing drought patterns across different temporal scales in Cyprus.

Statistical analyses

The gaps in the remote sensing time series were addressed using a Kalman smoothing filter for gap-filling and light smoothing (not for outlier detection per se) (Alavi et al. 2006). In addition to the Kalman smoothing filter (Moritz and Bartz-Beielstein 2017), moving average (MA) interpolation techniques were applied to address missing values. After evaluating the outcomes, the datasets completed using the Kalman smoothing filter were selected for subsequent time series analysis. To identify potentially influential observations, the Kalman smoothing filter was complemented with regression analysis using Cook's distance (Verbesselt et al. 2010).

Cook's distance (D) was employed as a diagnostic measure to assess the influence of individual observations on the fitted values from a preliminary fit. Specifically, for an observation i ($i = 1,\ldots, n$), Cook's distance Di represents the cumulative effect of excluding observation i on the fitted values, considering all other observations. Observations exceeding a pre-specified influence threshold were flagged for inspection. If a flagged point was judged as a measurement artefact (rather than a genuine extreme), it was replaced by the Kalman estimate and the series was re-estimated; otherwise, it was retained to preserve true extremes. All analyses were re-run after treatment and checked for robustness to inclusion/exclusion of flagged points (Cook and Weisberg 1982; Atkinson et al. 1997).

The Spearman correlation coefficients (ρ or *rho*), along with their corresponding p-values (p), were calculated to evaluate the possible responses of vegetation (based on indicators EVI, GPP, LAI, NBR, NDMI, NDVI, NDWI, and SAVI derived from remote sensing data) to meteorological drought (based on indicators SPI, SPEI, and PDSI). These potential relationships were assessed across various time periods, of annual, three-month (December–February, June–August), five-month (May–September) and six-month (October–March, April–September, May–October) duration for each year as well as across multiple years (2–10 past years), from 1990 to 2020. The above data were screened using 10 year running mean correlation analysis "window". This method provided an in-depth perspective of the impact that water availability can exercise on primary tree growth and on the state of tree foliage. It has also been applied to investigate similar impacts of drought on secondary tree growth under Mediterranean climatic conditions (Mazza and Sarris 2021; Sarris and Christodoulakis 2024). The Spearman's *rho* was specifically employed to also address potential non-normality in the data distribution. Highly statistically significant correlations were set at $p < 0.001$, and ranked by ascending p-values to highlight the most robust associations (Choi et al. 2013).

Running-mean and moving-window framework for vegetation-climate correlation analysis

To investigate the long-term dynamics of vegetation responses to drought, we first smoothed all datasets—including SPI, SPEI, PDSI, and remotely sensed vegetation metrics—using 10-year running means with a 1-year step; values are reported in terms of their window ranges, to emphasize the decadal context (e.g., 1992–2001, 1993–2002,…). Then we performed a correlation analysis for the period 1992–2017 (n = 17) for *J. phoenicea* and for the period 1992–2020 (n = 20) for *Q. alnifolia* and *P. brutia* using the Spearman's rank correlation coefficient (*rho*). The time span of analysis included both the period before tree mortality and the recovery of vegetation thereafter. Before correlations and transformation into 10-year running mean, all data were normalized by conversion into z-scores.

Building on this, we applied a 10-year moving "window" correlations analysis to explore temporal shifts in vegetation–climate relationships. Analyses used the annual, unsmoothed (but z-scored) series (i.e., no additional smoothing within windows), 10-year windows with a 1-year step. Annual vegetation indicators (EVI, GPP, LAI, NBR, NDMI, NDVI, NDWI, SAVI) were correlated on the one hand (X) with potential climatic drivers on the other hand (Y) derived from SPI, SPEI, and PDSI for the period 1992 to 2020 provided 20 correlation coefficients from each 10-year analysis "window" for each (X, Y) pair (EVI vs. SPI, GPP vs. SPI…SAVI vs. SPI etc. with 1992–2001 as "window" number one, and 2011–2020 as "window" number 20). Considering all three drought indicators this added up to 60 correlations per vegetation indicator. However, each drought indicator produced 16 different potential climatic drivers. These were classified as: (A) Monthly and seasonal climate (three-month i.e., December–February, June–August; five-month i.e. May–September; six-month e.g., October–March, April–September, May–October). (B) Annual climatic conditions (January–December and (C) Multi-year accumulations. For (C), we evaluated rolling windows of 2–10 years: 2-year windows (1992–1993, 1993–1994,…), 3-year windows (1992–1994, 1993–1995,…), up to 10-year windows (1992–2001, 1993–2002). Thus, within each 10-year correlation analysis "window" an annual (January–December) vegetation indicator produced 16 correlation coefficients from being correlated with the climatic drivers of SPI, or 320 (16×20) for the entire 1992–2020 period of analysis. Considering SPEI and PDSI as well, this method produced 960 correlation coefficients in total per vegetation indicator or 7680 correlation coefficients in total from all vegetation indicators per site. In other words, each of the 8 vegetation indicators produced 320 correlation coefficients per site. Correlations were not adjusted for autocorrelation.

To place these results in the context of drought events, each 10-year moving "window" was overlaid with background shading representing standardized SPEI (z-score) values. Red hues indicate increasing drought severity (SPEI < 0), while blue hues represent wetter-than-average conditions (SPEI > 0). SPEI values are divided into six discrete color bins, with threshold breaks evenly spaced between 0 and the observed maximum absolute SPEI value for each area. This results in site-specific transitions that dynamically scale with local SPEI variability, with full SPEI time series per site shaded into six discrete bins 0, ±0.4, ±0.8, ±1.2, ±1.6, ±2.0. The analysis was designed to test vegetation responses to climate during drought periods associated with tree mortality for specific species (2008 for *P. brutia* and *Q. alnifolia*, and 2016 for *J. phoenicea*), as well as to compare with other drought or wet periods where mortality was not observed.

Results

Assessment of meteorological drought indicators and their ecological impacts

Across all study areas, the timing of extreme drought conditions appears to align closely with known episodes of tree mortality, supporting a potential causal link.

The analysis of drought indicators for *J. phoenicea* at the Akamas site highlights moderate and severe drought events from 1995 to 2018, with Fig. 6a. Based on the PDSI, moderate droughts (PDSI < −2.5) occurred in 2004–2005, 2006, 2008, 2010, and 2014. SPEI indicated moderate drought conditions (SPEI < −1) in 1995, 2005–2008, and 2014. Similarly, SPI also captured drought anomalies (SPI < −1) during 2005–2008 and 2014, with the details presented in Fig. 6a. However, the most severe drought occurred in 2016, with extreme values recorded across all three indicators (SPI and SPEI < −2 and PDSI < −5). Specifically, the SPEI reached −2.63 in November, while the SPI dropped to −2.71, in the same month. Notably, the PDSI revealed even more prolonged stress, with values dropping to −6.04 in June, −5.78 in May, −5.47 in July, and −5.02 in August, which is shown in Fig. 6a. These patterns indicate that drought conditions were severe throughout the dry season and coincide with the mortality observed for *J. phoenicea* the same year in Akamas (Fig. 3; see Supplementary Table S1).

In Machairas site (*Q. alnifolia*), moderate drought conditions were observed in 1995, 2014, and 2018 as per the PDSI. Additionally, the SPEI detected moderate droughts in 1995, 1998, 2000, 2013, 2014, and 2016, while SPI anomalies pointed to moderate drought years in 1995, 1997, 1998, 2013, 2014, and 2016, with prolonged moderated drought conditions emerging in 2018. However, 2008 marked a peak in atmospheric drought stress, with sustained low values for PDSI, SPEI, and SPI, highlighted in Fig. 6b). In 2008, PDSI reached −4, while the lowest SPEI was −2.15 in September, followed by −2.12 in August and −2.12 in October. SPI values corroborate this, reaching −2.44 in October, −2.42 in September, and −2.38 in August. These extreme drought conditions are supportive of the mortality events recorded in *Q. alnifolia* populations in 2008 in Machairas forest (Fig. 4; see Supplementary Table S1).

At the Stavrovouni site (*P. brutia*), moderate drought occurred in 1995–1996, 2013–2014, and 2016–2018 according to the PDSI. SPEI detected moderate droughts in 1995, 2000, 2006, 2013, 2014, and 2016, while SPI indicated similar drought signals in 1995, 2006, 2013, 2014, and 2016, with Fig. 6c highlighting these events. Year 2008 stands out, with the SPEI dropping as low as −2.84 in August, −2.84 in July, and −2.80 in May. SPI followed a similar pattern, with its most severe value of −3.49 in May, alongside −3.44 in June and −3.41 in July. PDSI values further confirm extreme

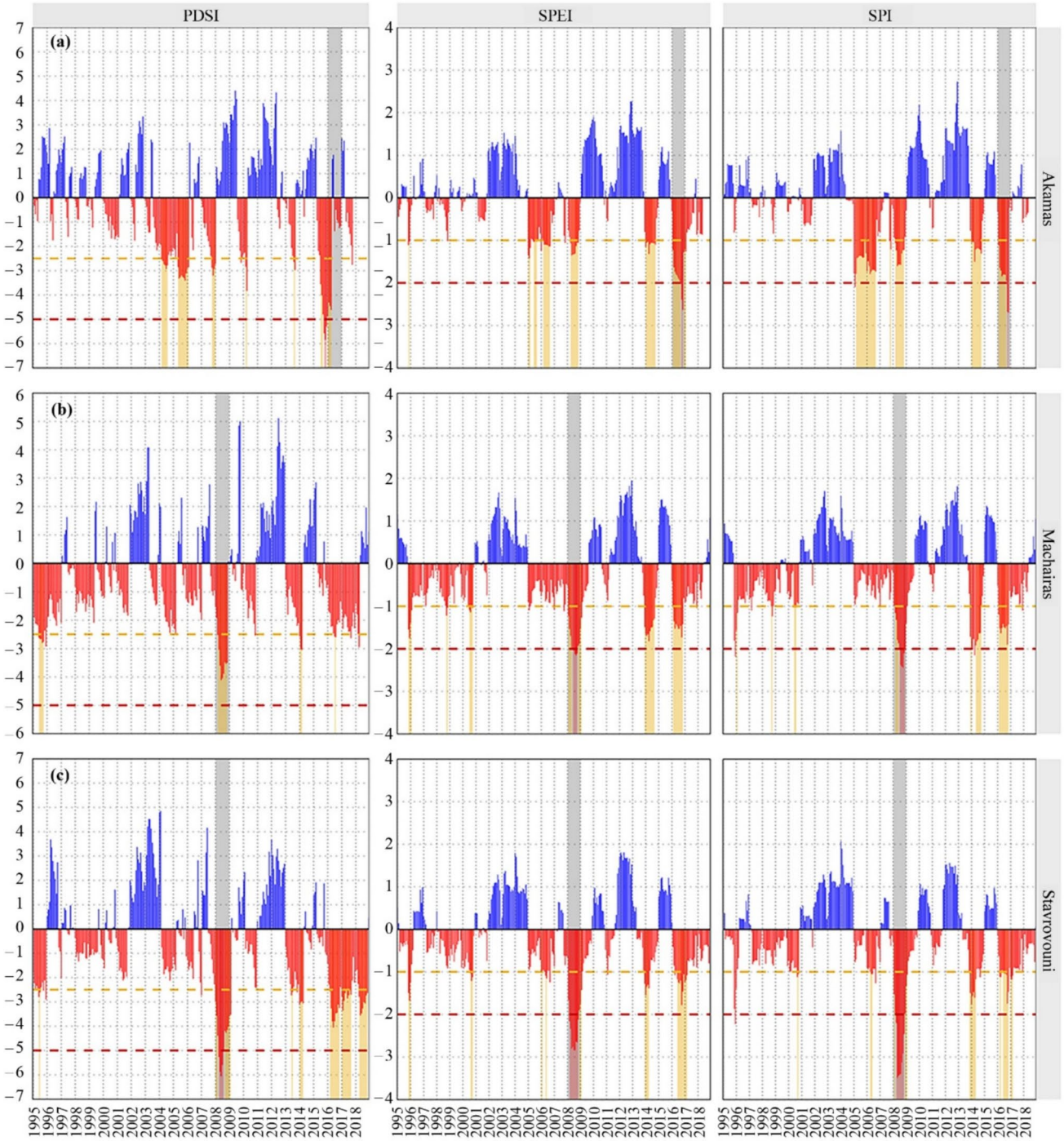

Fig. 6 Drought variability at three sites in Cyprus (1995–2018). Columns show PDSI-12, SPEI-12 and SPI-12; rows correspond to Akamas (**a**), Machairas (**b**) and Stavrovouni (**c**). Yellow shading indicates moderate drought (PDSI < −2.5; SPEI/SPI < −1) and red shading indicates severe drought (PDSI < −5; SPEI/SPI < −2). Grey shading marks years with observed mortality (Machairas: 2008; Stavrovouni: 2008; Akamas: 2016)

drought for 2008: −6.06 in June, −5.88 in May, −5.59 in July, −5.27 in April and −5.02 in August. The severity of drought is in line with *P. brutia* desiccation and subsequent dieback observed in Stavrovouni forest in 2008 (Fig. 5; see Supplementary Table S1).

Long-term vegetation dynamics explained by drought indicators

For *J. phoenicea* the best correlations ($p < 0.001$) between drought indicators and indicators for vegetation conditions

provided by remote sensing smoothed by conversion into 10-year running means appeared between SPI and NBR (*rho* = 0.86), between SPEI and NDMI (*rho* = 0.80) and between SPI and NDWI (*rho* = −0.72) (Table 1). PDSI produced significant correlations only with NBR and NDVI (*rho* = 0.60; *rho* = 0.52), but at lower significance ($p < 0.05$). Since NBR produced a significant correlation also with SPEI at $p < 0.01$, it was the only indicator providing significant correlations with all three drought indicators. For *Q. alnifolia*, correlations were significant between SPI or SPEI and NDWI at $p < 0.05$ (*rho* = −0.35; *rho* = −0.37), whereas for PDSI, in some cases where higher correlations were obtained, their sign was opposite to what would be logically expected and thus they cannot be considered credible. For *P. brutia*, PDSI appeared as the best predictor. Correlations between PDSI and NBR (*rho* = 0.84), or PDSI and NDMI (*rho* = 0.84) were very highly significant ($p < 0.001$). NBR also produced significant correlations with SPI (*rho* = 0.57; $p < 0.01$), while for SPEI its best correlation was with SAVI (*rho* = 0.57; $p < 0.01$) (Table 1).

Table 1 Spearman's *rho* between three drought indices (SPI, SPEI and PDSI) and eight remote-sensing vegetation indicators for each tree species. Time series were smoothed using 10-year running means before correlations were calculated. Results are shown for 1992–2017 (n = 17) for *J. phoenicea* and for 1992–2020 (n = 20) for *Q. alnifolia* and *P. brutia*. Asterisks indicate that the correlation is statistically different from zero using a two-tailed test (* for $p < 0.05$; ** for $p < 0.01$; *** for $p < 0.001$). Bold italics mark the strongest association (largest p) among the vegetation indicators for a given species, and bold marks the second strongest

	Remote sensing indicator	Drought indicator		
		SPI	SPEI	PDSI
Juniperus phoenicea	***NDMI***	0.64**	**0.80*** **	0.34
	EVI	0.60*	0.32	0.40
	GPP	0.65**	0.46	0.43
	LAI	0.60*	0.32	0.40
	NBR	**0.86*** **	0.65**	0.60*
	NDVI	0.71**	0.32	0.52*
	NDWI	**−0.72*** **	−0.72**	–0.42
	SAVI	0.61**	0.35	0.41
Quercus alnifolia	NDMI	0.25	-0.04	−0.47*
	EVI	0.36	0.11	−0.44
	GPP	0.32	0.13	−0.50*
	LAI	0.33	0.13	−0.50*
	NBR	0.22	-0.08	−0.50*
	NDVI	0.32	0.23	−0.31
	NDWI	−0.35	−0.37	0.05
	SAVI	0.37	0.17	−0.48*
Pinus brutia	***NDMI***	0.52*	0.22	**0.84*** **
	EVI	0.10	0.23	–0.41
	GPP	0.01	0.18	–0.49*
	LAI	0.17	0.30	–0.35
	NBR	0.57**	0.23	**0.84*** **
	NDVI	0.55*	0.49*	0.25
	NDWI	–0.24	–0.39	0.31
	SAVI	0.50*	0.57**	0.09

On the one hand, for the two conifer species, NBR is the most accurately described indicator by the drought indicators based on SPI and PDSI, followed by NDMI, which is better described by PDSI and SPEI. On the other hand, no drought indicator alone appears to fully capture the long-term trends of the vegetation indicators. For the evergreen broadleaf none of the eight indicators tested appears to satisfactory capture long-term trends in climate, as shown in Fig. 7.

Correlations between remote sensing and meteorological drought indicators per decade

Following the analysis of long-term trends, we conducted a more detailed temporal assessment to resolve the timing and consistency of these relationships within each decade: we applied a detailed moving-window correlation analysis, using annual remote sensing indicators of vegetation, along with various temporal formulations of drought indicators, as explained below.

In the first step, we calculated the frequency (count) of the highest correlation coefficients for each vegetation indicator X across every 10-year analysis window (as described above). This provided a preliminary measure of which remote sensing vegetation indicators were most sensitive to SPI, SPEI, or PDSI, and potentially more effective in explaining forest decline and mortality (Spearman's $|rho| > 0.881$; $p < 0.001$; Fig. 8). Both conifer species (*J. phoenicea* and *P. brutia*) produced much better results than the ever-green broadleaf (*Q. alnifolia*). *J. phoenicea* at Akamas exhibited the highest number of significant correlations, with most coming from NDMI, NBR, and NDWI, suggesting that the species' foliage is highly responsive to drought effects. *P. brutia* at Stavrovouni was similarly sensitive and showed a very strong signal for NBR, followed by NDMI and NDWI. *Q. alnifolia* at Machairas showed comparatively low sensitivity, with fewer significant correlations than those observed for the conifers. Of the tested indicators, NDMI, NDWI, and NDVI exhibited the most consistent responses, as presented Fig. 8.

In the second step, we calculated the frequency (count) of the highest correlation coefficients for each climatic driver Y across every 10-year analysis window (as described above). This provided a preliminary measure of which variations of the meteorological drought indicators—ranging from seasonal to multi-year scales, and derived from SPI, SPEI, or PDSI—acted as drivers of vegetation indicator variability and were potentially more

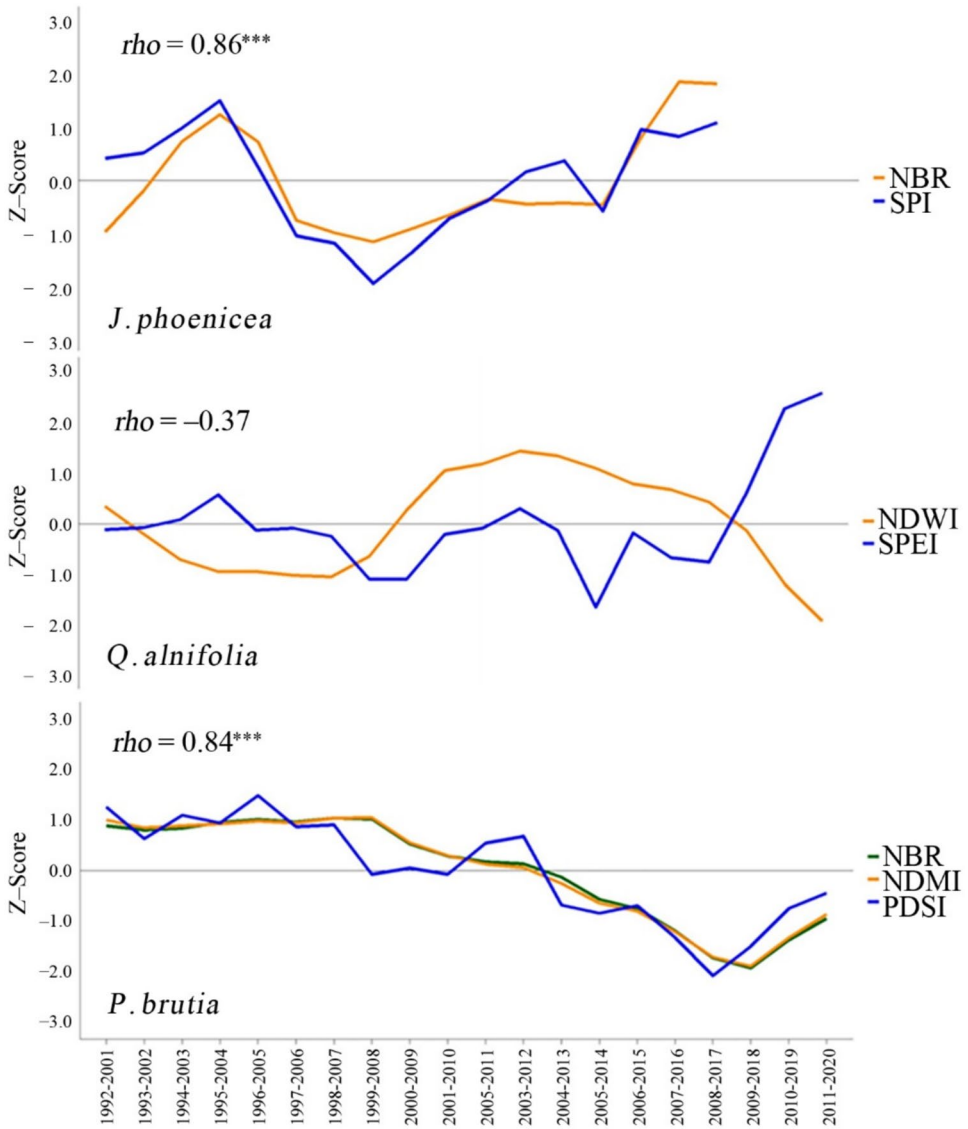

Fig. 7 Best correlating indicators for the condition of vegetation and climate smoothed by conversion into 10-year running means per tree species based on Table 1. Asterisks indicate significance levels at $p < 0.05$ (*), $p < 0.001$ (***)

effective in explaining forest decline and mortality, illustrated in Fig. 9.

The vegetation of *J. phoenicea* in Akamas appeared to be most sensitive to 2-year climatic conditions, followed by climate of the past 3 to 4 years. NDWI, NBR, NDMI and NDVI were the best vegetation indicators correlated with the above climatic drivers. For the ever-green broadleaf *Q. alnifolia* in Machairas, the past 6- to 7-year climate appeared to be a key driver for the condition of its foliage. NDVI, NDMI, EVI and NDWI were the best vegetation indicators correlated with the above climatic drivers, although the effects were less strong compared to the conifers. For the *P. brutia* in Stavrovouni, the correlations of the past 3- to 6-year climate with tree crown conditions were the most robust. NBR, NDWI, NDMI, and SAVI were the best vegetation indicators correlated with the above climatic drivers.

As a third step, for each tree species the best correlation coefficients ($|rho| > 0.881$; $p < 0.001$) per vegetation indicator, as identified during the first step of analysis, were plotted in relation to their best climatic predictors, produced either from SPI, SPEI or PDSI for each 10-year analysis "window", depicted in Fig. 10. Figure 10 shows only the three dominant indicators with the best-performing 10-year windows, Akamas duration = 2; Machairas duration = 6; Stavrovouni duration = 4 (the full set of results is provided in Supplementary Figs. S1–S3).

At Akamas site (*J. phoenicea*), decades 2007–2016 and 2008–2017 (Supplementary Fig. S1) include vegetation responses related to the mortality of 2016, representing conditions that vegetation experienced mostly before and during the event. All three remote sensing vegetation indicators (NDMI, NBR, NDWI) agree that the climatic drivers for vegetation responses within the decades 2007–2016 and

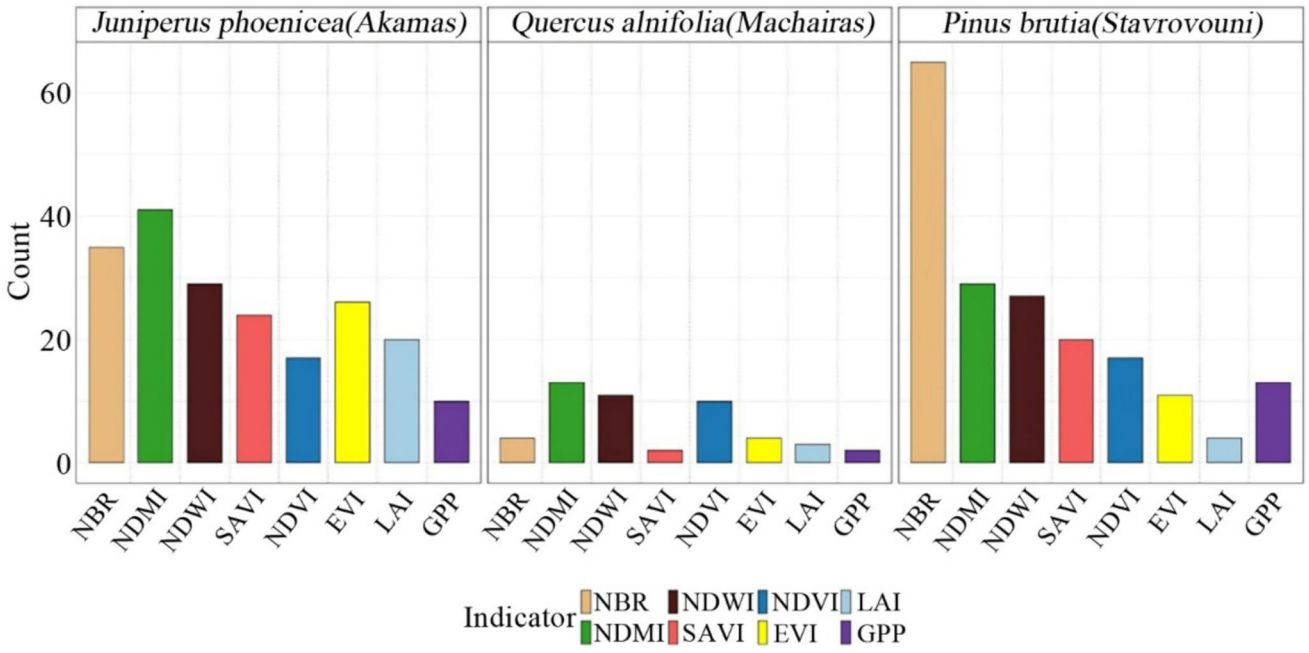

Fig. 8 Classification of correlation coefficients from correlating potential climatic drivers for vegetation based on drought indicators (from seasonal to multiple year for either SPI, SPEI or PDSI) with tree crown conditions (vegetation indicators). The coefficients were grouped based on the remotely sensed vegetation indicator they represent, for species **a** *Juniperus phoenicea*, **b** *Quercus alnifolia*, and **c** *Pinus brutia*. The frequency (count) represents how many coefficients were significant at $p < 0.001$ per vegetation indicator

2008–2017, were related to antecedent climatic conditions spanning 4–5 years (including the year of monitoring). This is in contrast to the past period of drought centered around 1999–2008, (Fig. 10) where again all remote sensing indicators for vegetation suggest that the climatic drivers for vegetation responses were linked to conditions from the preceding 2 years (Fig. 10) (including the year of monitoring) or to winter/wet season climate (Dec–Fed or Oct–Mar for NDMI and NBR) (Supplementary Fig. S1). Overall, prior to the 2016 drought event, vegetation responses in Akamas appear to have been influenced mainly by seasonal factors or antecedent climatic conditions over the previous 2–3 years, with SPI identified as the most consistent drought indicator (Fig. 10). However, during the period of observed *J. phoenicea* mortality the past 4 and 5 years of climate (precipitation) drove vegetation responses.

At Machairas site (*Q. alnifolia*), decades from 2004–2015 till 2008–2017 (Supplementary Fig. S2; Fig. 10) include vegetation responses related to the mortality of 2008 for NDMI, NDVI and NDWI (Fig. 10) (including 2002–2011 but only for NDWI), representing conditions that vegetation experienced primarily during and after the mortality event (Supplementary Fig. S2; Fig. 10). All the above remote sensing indicators agree that the climatic drivers for vegetation responses from 2004–2015 till 2008–2017, were related to 5, 6 and 7 years of past climate (including the year of monitoring). Overall, the ability of the remote sensing vegetation indicators tested, to identify responses of vegetation to climate before the tree mortality event of 2008 remains poor for the evergreen *Q. alnifolia*. It is when years of reduced vegetation density because of *Q. alnifolia* dieback are included (e.g., 2009 and thereafter) that correlation signals became significant, and were related to the SPI, and SPEI (Stefanidis et al. 2023) drought indicators.

At Stavrovouni site (*P. brutia*), decades from 1999–2008 till 2004–2013 (Supplementary Fig. S3) include vegetation responses related to the mortality of 2008 for NDMI, NBR and NDWI (Fig. 10), representing conditions that vegetation experienced in the years surrounding the 2008 event (Supplementary Fig. S3; Fig. 10). However, NDWI signals also cover the periods of recovery from 2005–2014 till 2008–2017 (Fig. 10), which, to a smaller extent, are also evident in NDMI signals (2005–2014 and 2006–2015). NDMI and NBR remote sensing indicators show that vegetation responses during 1999–2008 to 2004–2013 were driven by antecedent climate variability over the prior 4–6 years, including the monitoring year. In contrast, NDWI signals were primarily associated with 2–3 years of preceding climatic conditions during the same period. For NDWI, associations with 4–5 years of earlier climate influences emerged during the recovery phases from 2005–2014 to 2008–2017. Relative to the pre-2008 drought period, 4–5 years of previous climate variability provided a better explanation of vegetation responses, shifting to 6 years once the 2008 drought

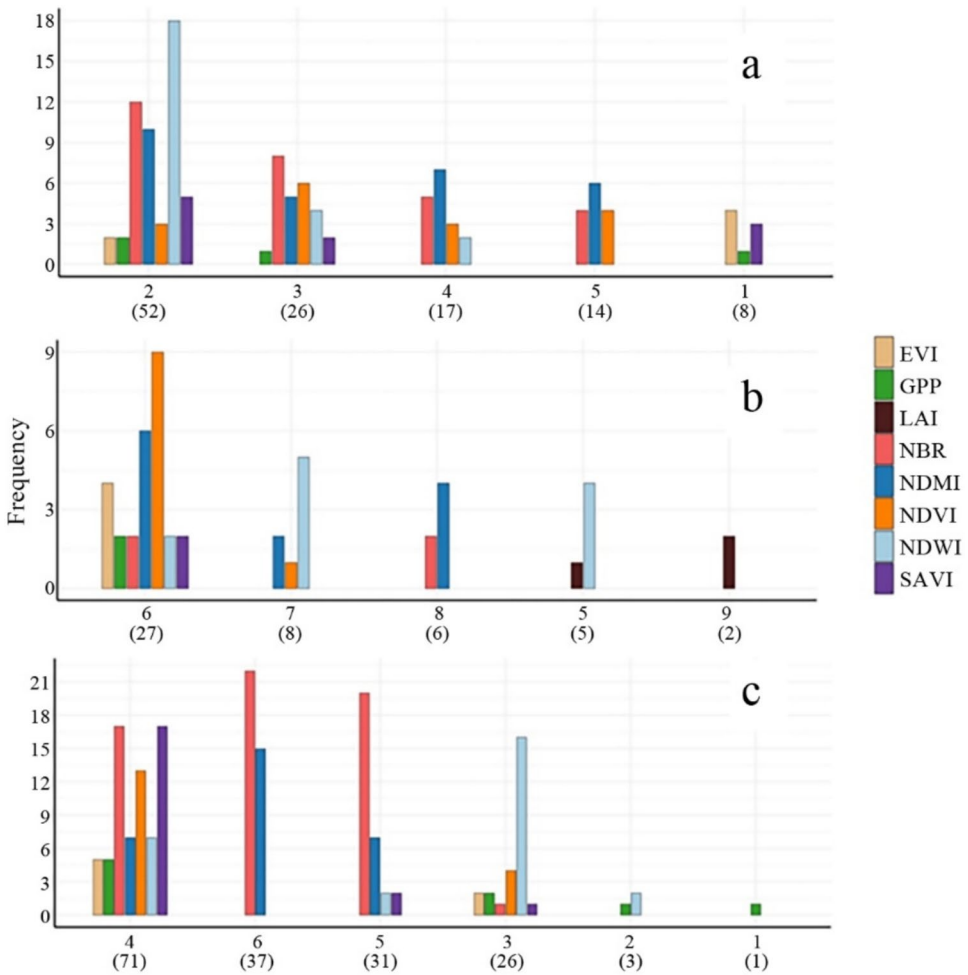

Fig. 9 Classification of correlation coefficients from correlating potential climatic drivers for vegetation based on drought indicators SPI, SPEI and PDSI with tree crown conditions (vegetation indicators). The coefficients were grouped based on the duration of the climatic driver they represent (e.g., 1 = co-occurring climatic conditions to the year of vegetation monitoring; 7 = climate of the past 7 years including climatic conditions co-occurring within the year of vegetation monitoring) for species **a** *Juniperus phoenicea* (Akamas), **b** *Quercus alnifolia* (Machairas), and **c** *Pinus brutia* (Stavrovouni). The frequency represents how many coefficients were significant at $p < 0.001$ per vegetation indicator. In parenthesis is the total number of significant coefficients per climatic driver

occurred, as indicated by NDMI. For NBR and NDWI, no significant shift was detected.

Overall, out of the remote sensing vegetation indicators tested for the Pinus species, NDMI appears to be the most sensitive to climatic variability, producing signals related to the climatic drivers for vegetation responses before the 2008 drought, during its onset and for the period of recovery, based on all three drought indicators tested (i.e., SPI, SPEI and PDSI). NBR produced the highest correlations with the climatic drivers based mostly on SPI and SPEI for the period centered around the 2008 drought, with NDWI being better in capturing signals related to vegetation recovery based mostly on SPEI.

Discussion

Drought thresholds and vegetation indicators' response to tree mortality

Tree mortality is a key factor influencing forest functions and dynamics, with gymnosperms having been found to display different behavior than angiosperms trees. In this respect, generalized hydraulic failure related to drought and/or bark beetle outbreaks can be involved in the process (Cailleret et al. 2017). Our findings clearly outline that both the 2008 and the 2016 mortality events for the gymnosperms *P. brutia* and *J. phoenicea*, on the one hand, and for the angiosperm *Q. alnifolia*, on the other hand, at the xeric limits of their natural distribution range in Europe can be related to the very severe drought conditions (PDSI-12 < −5, SPI-12 and SPEI–12 < 2) that occurred within the dry season that mortality was observed (Figs. 3, 4, 5). It is a question whether these drought thresholds can be used to predict dryland forest mortality. For instance, values < 2 for the SPEI-12 time-series have been associated with mortality for the gymnosperm *P. halepensis* in the Eastern Mediterranean (Dorman et al. 2013, 2015a, b).

The vegetation indicators best explaining long-term vegetation dynamics appear to be different for the two conifer (gymnosperm) species investigated, compared to the evergreen broadleaf species (angiosperm), when including the period before the mortality events of 2008 and 2016 and the first years thereafter (Table 1; Figs. 7, 8). For *J. phoenicea*

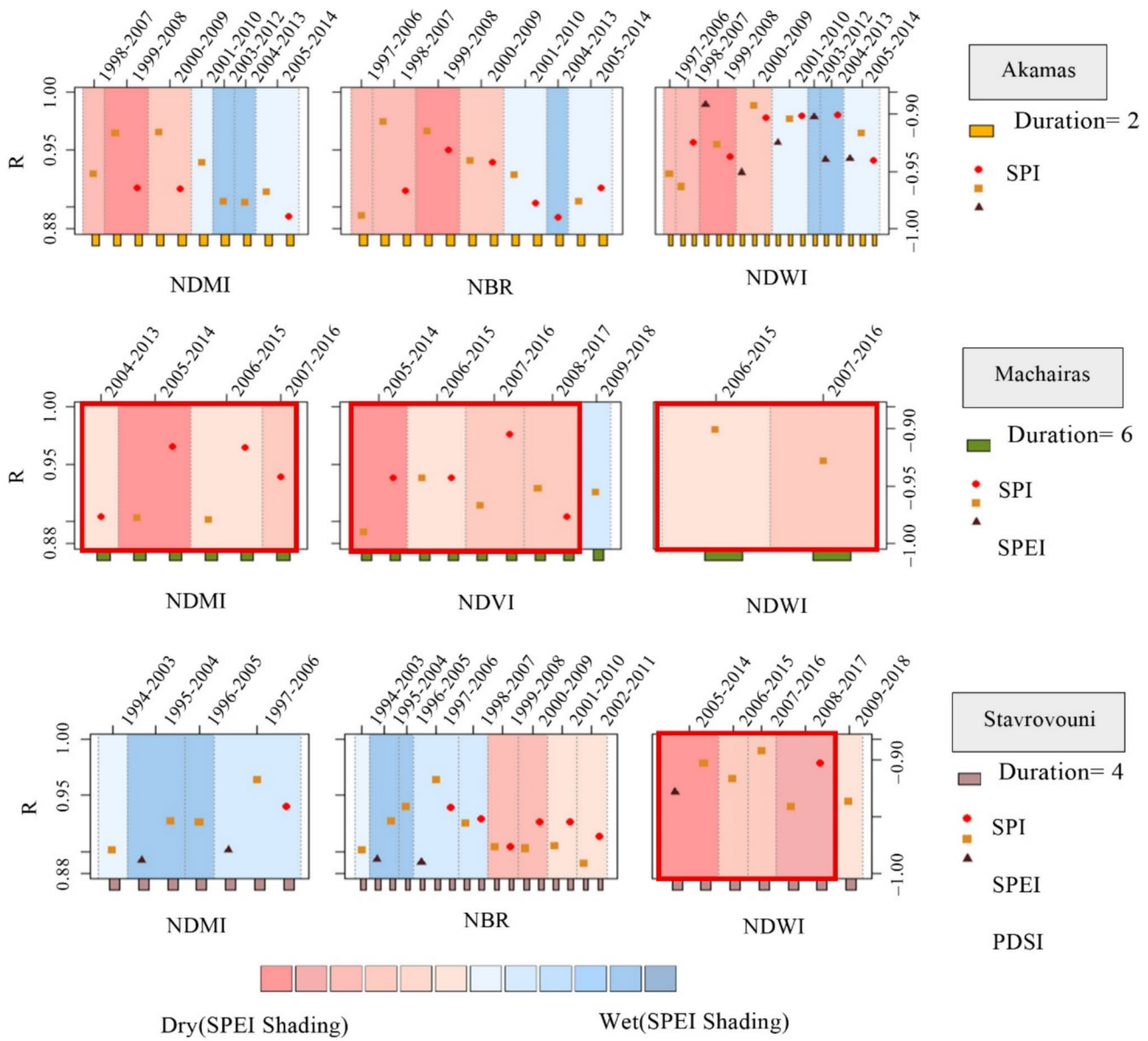

Fig. 10 The three remote sensing vegetation indicators with the strongest correlations (Spearman's $|rho| > 0.881$, $p < 0.001$, $n = 10$) with climate variability per decade for a wide range of potential climatic drivers (legend to the right). The small colored boxes at the bottom of each graph represent the climatic drivers that can explain the variability in vegetation conditions. Red boxes mark the time periods related to the mortality events. Events were in 2016 for *J. phoenicea* at the Akamas site; 2008 for *Q. alnifolia* at the Macheras site; and 2008 for *P. brutia* at the Stavrovouni site

and *P. brutia*, the Normalized Burn Ratio (NBR) appears as the remote sensing indicator most significantly connected with climatic variability as described by the SPI for the *J. phoenicea* and by the PDSI for the *P. brutia*. The Normalized Difference Moisture Index (NDMI) is the second most accurate indicator describing the long-term response of vegetation to SPEI for the *J. phoenicea*, and to PDSI for *P. brutia*.

However, when looking into the intra-decadal responses of vegetation to climatic variability, using our 10-year moving "window" correlation analysis, the NBR appears weaker during the decades that include the *J. phoenicea*' 2016 mortality event (2007–2016, 2008–2017). In this case, NDMI appears better than the NBR in explaining *J. phoenicea* vegetation's response to drought induced mortality. Nonetheless, the NBR performed exceptionally well, as did the NDMI, during the driest decades on record for the *J. phoenicea* Akamas site (e.g., 1998–07, 1999–00) coinciding, on the one hand, with the lowest decadal NBR-SPI values, and, on the other hand, with the lowest decadal NBR-SPEI

values in our time series (Fig. 7). It is worth noting that this is a time period when small scale mortality has been observed for Akamas *J. phoenicea* (see Supplementary Table S1). The NBR also produced very strong signals for *P. brutia*, but only during the early decades that involved the *P. brutia* 2008 mortality event (1999–2008 till 2004–13). Leaf structure and lifeform differ between the two conifer types (needle leaves for pines trees vs. scaly leaves for juniper shrubs). Nonetheless, during multi-year droughts (e.g., 2005–2009), conifer leaves can turn brown (Körner et al. 2005; Sarris et al. 2007). In these conditions leading to conifer dieback, both conifer types produce similar vegetation responses, which can be detected in the shortwave infrared bands, as indicated by the NBR and the NDMI. Healthy green vegetation will have a high NBR value. In contrast, burnt vegetation—similar to dry, brown vegetation or bare soil—shows a low NBR value (Digital Earth Australia 2025).

The most commonly used indicator in mortality detection is the NDVI (Xue and Su 2017), applied in ca. one-third of studies globally (Eliades et al. 2024). For our conifers, its performance was very poor when the entire time span of analysis is considered (i.e., 1990–2020; see Table 1 and Fig. 8). These findings are in agreement with a study on the mortality of Pinus pinaster in southern Spain where the NBR and the NDMI provided the highest correlations with defoliation rates and needle desiccation compared to the NDVI (Ariza Salamanca et al. 2019). For mapping defoliation, it has been shown that shortwave infrared reflectance (SWIR bands), on which the NBR and the NDMI are based on, work better than the visible-near infrared indices that are used in the NDVI (Townsend et al. 2012). To the contrary, the NDVI may be more accurate under conditions representing severe or complete defoliation processes (Marx and Kleinschmit 2017). This may explain why the NDVI (together with SAVI) appears to outperform NBR from 2005–2014 till 2008–2017, i.e., when post mortality years with high rates of defoliation are included in the analysis for *P. brutia* (see Supplementary Table S2).

Furthermore, the evergreen *Q. alnifolia* in our study produced much better correlations with the climatic indices when monitored using the NDVI compared to the NBR (Figs. 8, 10). In contrast to conifers, where dead leaves can be retained on the tree for many years, broadleaves/angiosperms shed their dead foliage at a much faster pace (Reyer et al. 2013; Zhang et al. 2020). Thus, *Q. alnifolia* likely grants NDVI higher accuracy by experiencing faster, more severe defoliation than the conifers (Italiano et al. 2024). Evidence shows that NDVI can distinguish healthy from declining trees (Aguilar et al. 2012) with studies in *Q. suber* woodlands further demonstrating its strong correlation with dieback severity (Bambagioni et al. 2025). However, this accuracy was reduced in dense forests or for overlapping oak canopies (Cook and Weisberg 1982; Aguilar et al. 2012). The *Q. alnifolia* vegetation we monitored was actually quite dense (Fig. 4). This may explain why the NDVI did not prove effective in capturing the responses of vegetation to climate before 2008 when severe mortality occurred. Thereafter, the vegetation density of surviving oaks would be expected to be much lower, permitting the NDVI to capture the responses of oak vegetation to climate. However, further research is needed to accurately monitor the status of *Q. alnifolia* defoliation under severe drought together with the density of surviving stands coupled with remote sensing to confirm our hypothesis.

From resilience to mortality: insights from the multi-year correlations

During the period that tree mortality was observed, primary productivity of all three tree species investigated appears to have been related to climatic conditions that occurred not only during the year that trees were desiccated. It was clearly related to climate several years before the year that trees died. For *J. phoenicea* in Akamas site, during the first decade that included the 2016 tree mortality event, the past 4 and 5 years of precipitation drove vegetation responses, having shifted from seasonal or climate of the past 2 to 3 years, i.e., the climate that appears to have been driving primary productivity the decades before 2016. For *Q. alnifolia* at Machairas site, decadal vegetation responses coinciding with the tree dieback of 2008 (from 2004–2015 till 2008–2017) were found to be related to 5, 6 and 7 years of preceding climatic conditions (including the year of mortality). For *P. brutia* at Stavrovouni site, the climatic drivers for vegetation responses for the time period from 1999–2008 till 2004–2013, related to the 2008 *P. brutia* mortality event, were primarily related to 4, 5 and 6 years of past climate (including the year of tree desiccation). Such long-term influences of climate have been attributed to the utilization by deep tap roots of moisture stored underground within the critical zone, sustaining tree life in drylands (Sarris and Christodoulakis 2024). However, our study does not include direct measurements of soil moisture, groundwater levels, or plant water sources. Therefore, the role of deeper, root-accessible water stores is discussed here as a plausible mechanism consistent with the observed multi-year vegetation-climate associations, rather than as a demonstrated causal driver. These moisture reserves are refilled over several years of rainfall, while their depletion makes tree survival under extreme drought very challenging (Sarris and Mazza 2021a; Sarris and Christodoulakis 2024). Only the decadal vegetation responses of *J. phoenicea* coincided with seasonal drought periods, particularly related to the wet season months (December–February, October–March) e.g. during 1999–2008, 2000–2009. This indicates that *J. phoenicea* was responding not only to cumulative water deficits but also

to acute seasonal shortages. The above pattern suggests the species' reliance on surface and mid-depth water sources at the site investigated. On the other hand, the deep root system of *Q. alnifolia* appears to buffer short- to mid-term drought impacts (Kolb and Stone 2000; Bello et al. 2019; Moreno-de-las-Heras et al. 2023). This species typically manifests signs of drought stress only under sustained and severe conditions, without displaying early indicators during the initial stages of soil moisture decline as has also been suggested for *Q. ilex* (Peguero-Pina et al. 2023).

Our findings on the climatic signals that are related to primary growth and mortality of dryland trees, monitored via remote sensing, are in agreement with results that have been based on secondary growth using ground based dendrochronological methods as mentioned in the literature above. However, although the phenomenon is not observed for the first time, it is the first time that it has been captured based on primary productivity and by using satellite remote sensing of vegetation. Past detection has been based on monitoring secondary growth (tree rings) using dendrochronological methods. These methods can be biased by the statistical tools used to interpret the annual radial increment of trees (Mazza and Sarris 2021). An independent approach based on satellite remote sensing provides an additional, independent line of evidence that is consistent with a storage-mediated 'memory' effect, whereby multi-year moisture deficits may contribute to elevated mortality risk under extreme drought in semi-arid forests. This reading is plausible in light of regional evidence from the Eastern Mediterranean—tree-ring and stable-isotope studies documenting multi-year climate controls and species-specific rooting strategies (Sarris et al. 2007, 2013). Moreover, the strong performance of moisture- and disturbance-sensitive indicators support their ability to detect delayed canopy responses associated with sub-lethal stress (Sheil 2018), which, although not immediately lethal, progressively reduce tree vigor and increases vulnerability to subsequent climatic extremes (Ariza Salamanca et al. 2019) potentially linked to progressive depletion of deeper, plant-accessible moisture within the critical zone.

In summary, and as a direct outcome of our research, a major achievement will be the delineation of high-risk areas using the most effective indicators identified in our analysis to improve predictions of areas vulnerable to mortality; subsequently, strengthening this tool through the development of an innovative indicator with stronger correlations will enable more reliable detection of tree mortality.

Conclusion

Our findings clearly outline that very severe drought conditions below the −2 thresholds for the SPI-12 and the SPEI-12, or −5 for the PDSI-12, exceed the capacity of *J. phoenicea*, *P. brutia* and *Q. alnifolia* to sustain healthy stands in Cyprus i.e., at habitats representing the xeric limits of their natural distribution range in Europe. Very low precipitation appears as the driving force of the phenomenon. However, starting from the year of drought induced mortality and including the years that followed, we identified that the annual response of these species' vegetation to such events was related to climate averaged over 4 to 7 past years (including the year of monitoring) depending on plant species. In these ecosystems, the annual variability of leaf browning and defoliation is consistent with long hydrological and/or ecological cycles. To our knowledge, this is the first remote-sensing-based assessment documenting robust multi-year associations between canopy condition and prior climate in these semi-arid forests. We interpret this pattern as a working hypothesis of a storage-mediated 'memory', potentially involving deeper, root-accessible moisture within the critical zone as surface pools are depleted during drought. This remains an inference from remote-sensing indicators rather than a direct observation of subsurface water storage.

Furthermore, our findings stress that the NBR and NDMI were significantly connected with climatic variability, as described by the SPI or SPEI for the *J. phoenicea* and by the PDSI for the *P. brutia*, before and at the first years after mortality has occurred. After some years have passed since the year of mortality, our findings suggest that the decadal response of vegetation to climate variability was better described by the NDVI. It is most likely that these responses are related to the browning of conifer leaves at the first stages of drought impact, a phenomenon better captured by NBR. Moreover, severe defoliation that occurs some years after mortality affects the conifer stands appears to be better captured by the NDVI and to a lesser extent by the SAVI.

Yet, the dense stands of the evergreen *Q. alnifolia* seem to be difficult to monitor via the remote sensing vegetation indicators applied here. However, after mortality has occurred within *Q. alnifolia* stands the NDVI provides the highest accuracy. This is likely because the oaks experienced more severe defoliation than the conifers and at a faster pace, reducing their vegetation density at levels within which the NDVI can function. Furthermore, this endemic to Cyprus very deep-rooted oak likely has access to deep moisture pools within the critical zone of the habitats investigated, permitting high resilience to moderate drought. This in turn does not appear to produce early signals of stress detectable via satellite remote sensing. However, further research is needed to explore the above hypothesis.

Overall, this study presents a novel and comprehensive analysis, undertaken for the first time, by combining remote sensing-derived with meteorological drought indicators at long-term scales, to characterize tree mortality. By capturing severe drought events and cumulative moisture deficits together with their ecological consequences, our approach provides key insights for regional drought assessment and

long-term ecosystem monitoring. It underscores the critical importance of distinguishing between gymnosperm from angiosperm vegetation dynamics when assessing drought impacts on forest ecosystems. It also highlights the different detection capabilities of satellite remote sensing vegetation indicators in such ecosystems under severe drought stress, focusing on multi-year and remote sensing-based indicators to effectively track drought impacts. A deeper understanding of these complex interactions will inform drought mitigation strategies, enabling the incorporation of species-specific responses and long-term climatic trends into forest management and conservation planning in light of drought induced mortality that is expected to affect more severely forest ecosystems under climate change.

Acknowledgements The authors acknowledge the "EXCELSIOR": ERATOSTHENES: Excellence Research Centre for Earth Surveillance and Space-Based Monitoring of the Environment H2020 Widespread Teaming project (www.excelsior2020.eu, accessed on 1 July 2024). The "EXCELSIOR" project has received funding from the European Union's Horizon 2020 Research and Innovation Programme under Grant Agreement No 857510 from the Government of the Republic of Cyprus through the Directorate General for the European Programmes, Coordination and Development and the Cyprus University of Technology.

Author contributions Conceptualization and analysis, F.E.; Methodology, F.E., S.M., and D.S.; Results, F.E., S.M., and D.S.; Discussion, F.E., S.M., and D.S.; Resources, F.E.; Data curation, F.E.; Writing—original draft, F.E., S.M., and D.S.; Writing—review and editing, F.E., S.M., F.B., D.S., C.D., and D.H.; Visualization, F.E.; Supervision, F.B., C.D., and D.H.; Project administration, D.H.; Funding acquisition, D.H. All authors have read and agreed to the published version of the manuscript.

Funding Open access funding provided by the Cyprus Libraries Consortium (CLC).Funding Open access funding provided by the Cyprus Libraries Consortium (CLC).Funding Open access funding provided by the Cyprus Libraries Consortium (CLC).

References

Aguilar C, Zinnert JC, Polo MJ, Young DR (2012) NDVI as an indicator for changes in water availability to woody vegetation. Ecol Indic 23:290–300. https://doi.org/10.1016/j.ecolind.2012.04.008

Alavi N, Warland JS, Berg AA (2006) Filling gaps in evapotranspiration measurements for water budget studies: evaluation of a Kalman filtering approach. Agric for Meteor 141(1):57–66. https://doi.org/10.1016/j.agrformet.2006.09.011

Allen CD, Macalady AK, Chenchouni H, Bachelet D, McDowell N, Vennetier M, Kitzberger T, Rigling A, Breshears DD, Hogg EH, Gonzalez P, Fensham R, Zhang Z, Castro J, Demidova N, Lim JH, Allard G, Running SW, Semerci A, Cobb N (2010) A global overview of drought and heat-induced tree mortality reveals emerging climate change risks for forests. For Ecol Manag 259(4):660–684. https://doi.org/10.1016/j.foreco.2009.09.001

Alley WM (1984) The palmer drought severity index: limitations and assumptions. J Clim Appl Meteorol 23(7):1100–1109

Ariza Salamanca AJ, Navarro-Cerrillo RM, Bonet-García FJ, Pérez-Palazón MJ, Polo MJ (2019) Integration of a landsat time-series of NBR and hydrological modeling to assess *Pinus pinaster* aiton. forest defoliation in south-eastern Spain. Remote Sens 11(19):2291. https://doi.org/10.3390/rs11192291

Atkinson AC, Koopman SJ, Shephard N (1997) Detecting shocks: outliers and breaks in time series. J Econom 80(2):387–422. https://doi.org/10.1016/S0304-4076(97)00050-X

Bambagioni E, Anzilotti S, Borghi C, Chirici G, Salbitano F, Marchetti M, Francini S (2025) Satellite remote sensing for monitoring cork oak woodlands—a comprehensive literature review. Diversity 17(6):420. https://doi.org/10.3390/d17060420

Bello J, Hasselquist NJ, Vallet P, Kahmen A, Perot T, Korboulewsky N (2019) Complementary water uptake depth of *Quercus petraea* and *Pinus sylvestris* in mixed stands during an extreme drought. Plant Soil 437(1):93–115. https://doi.org/10.1007/s11104-019-03951-z

Boegh E, Soegaard H, Broge N, Hasager CB, Jensen NO, Schelde K, Thomsen A (2002) Airborne multispectral data for quantifying leaf area index, nitrogen concentration, and photosynthetic efficiency in agriculture. Remote Sens Environ 81(2–3):179–193. https://doi.org/10.1016/S0034-4257(01)00342-X

Buma B, Wessman CA (2011) Disturbance interactions can impact resilience mechanisms of forests. Ecosphere 2(5):art64. https://doi.org/10.1890/ES11-00038.1

Cailleret M, Jansen S, Robert EMR, Desoto L, Aakala T, Antos JA, Beikircher B, Bigler C, Bugmann H, Caccianiga M, Čada V, Camarero JJ, Cherubini P, Cochard H, Coyea MR, Čufar K, Das AJ, Davi H, Delzon S, Dorman M, Gea-Izquierdo G, Gillner S, Haavik LJ, Hartmann H, Hereş AM, Hultine KR, Janda P, Kane JM, Kharuk VI, Kitzberger T, Klein T, Kramer K, Lens F, Levanic T, Linares Calderon JC, Lloret F, Lobo-Do-Vale R, Lombardi F, López Rodríguez R, Mäkinen H, Mayr S, Mészáros I, Metsaranta JM, Minunno F, Oberhuber W, Papadopoulos A, Peltoniemi M, Petritan AM, Rohner B, Sangüesa-Barreda G, Sarris D, Smith JM, Stan AB, Sterck F, Stojanović DB, Suarez ML, Svoboda M, Tognetti R, Torres-Ruiz JM, Trotsiuk V, Villalba R, Vodde F, Westwood AR, Wyckoff PH, Zafirov N, Martínez-Vilalta J (2017) A synthesis of radial growth patterns preceding tree mortality. Glob Change Biol 23(4):1675–1690. https://doi.org/10.1111/gcb.13535

Carpenter SR, Turner MG (2000) Hares and tortoises: interactions of fast and slow variablesin ecosystems. Ecosystems 3(6):495–497. https://doi.org/10.1007/s100210000043

Choat B, Jansen S, Brodribb TJ, Cochard H, Delzon S, Bhaskar R, Bucci SJ, Feild TS, Gleason SM, Hacke UG, Jacobsen AL, Lens F, Maherali H, Martínez-Vilalta J, Mayr S, Mencuccini M, Mitchell PJ, Nardini A, Pittermann J, Pratt RB, Sperry JS, Westoby M, Wright IJ, Zanne AE (2012) Global convergence in the vulnerability of forests to drought. Nature 491(7426):752–755. https://doi.org/10.1038/nature11688

Choi M, Jacobs JM, Anderson MC, Bosch DD (2013) Evaluation of drought indices via remotely sensed data with hydrological variables. J Hydrol 476:265–273. https://doi.org/10.1016/j.jhydrol.2012.10.042

Cook BI, Smerdon JE, Seager R, Coats S (2014) Global warming and 21st century drying. Clim Dyn 43(9):2607–2627. https://doi.org/10.1007/s00382-014-2075-y

Cook RD, Weisberg S (1982) Residuals and influence in regression. Chapman and Hall, New York and London

Dakos V, Scheffer M, van Nes EH, Brovkin V, Petoukhov V, Held H (2008) Slowing down as an early warning signal for abrupt climate change. Proc Natl Acad Sci USA 105(38):14308–14312

Digital Earth Australia (2025) Burnt area mapping using Sentinel-2 data. https://knowledge.dea.ga.gov.au/notebooks/Real_world_examples/Burnt_area_mapping/. Accessed 22 Aug 2025

Dorman M, Perevolotsky A, Sarris D, Svoray T (2015a) The effect of rainfall and competition intensity on forest response to drought: lessons learned from a dry extreme. Oecologia 177(4):1025–1038. https://doi.org/10.1007/s00442-015-3229-2

Dorman M, Svoray T, Perevolotsky A, Moshe Y, Sarris D (2015b) What determines tree mortality in dry environments? A multi-perspective approach. Ecol Appl 25(4):1054–1071. https://doi.org/10.1890/14-0698.1

Dorman M, Svoray T, Perevolotsky A, Sarris D (2013) Forest performance during two consecutive drought periods: diverging long-term trends and short-term responses along a climatic gradient. For Ecol Manag 310:1–9. https://doi.org/10.1016/j.foreco.2013.08.009

Dubinin V, Svoray T, Dorman M, Perevolotsky A (2018) Detecting biodiversity refugia using remotely sensed data. Landsc Ecol 33(10):1815–1830. https://doi.org/10.1007/s10980-018-0705-1

Eliades F (2016) Tree mortality in Akamas, Cyprus

Eliades F (2008) Tree mortality in Machairas, Cyprus

Eliades F, Sarris D, Bachofer F, Michaelides S, Hadjimitsis D (2024) Understanding tree mortality patterns: a comprehensive review of remote sensing and meteorological ground-based studies. Forests 15(8):1357. https://doi.org/10.3390/f15081357

Forest Department of Cyprus (2008) Tree mortality in Stavrovouni, Cyprus

Gao BC (1996) NDWI—a normalized difference water index for remote sensing of vegetation liquid water from space. Remote Sens Environ 58(3):257–266. https://doi.org/10.1016/S0034-4257(96)00067-3

Hartmann H, Bastos A, Das AJ, Esquivel-Muelbert A, Hammond WM, Martínez-Vilalta J, McDowell NG, Powers JS, Pugh TAM, Ruthrof KX, Allen CD (2022) Climate change risks to global forest health: emergence of unexpected events of elevated tree mortality worldwide. Annu Rev Plant Biol 73:673–702. https://doi.org/10.1146/annurev-arplant-102820-012804

Hember RA, Kurz WA, Coops NC (2017) Relationships between individual-tree mortality and water-balance variables indicate positive trends in water stress-induced tree mortality across North America. Glob Chang Biol 23(4):1691–1710. https://doi.org/10.1111/gcb.13428

Hersbach H, Bell B, Berrisford P, Hirahara S, Horányi A, Muñoz-Sabater J, Nicolas J, Peubey C, Radu R, Schepers D, Simmons A, Soci C, Abdalla S, Abellan X, Balsamo G, Bechtold P, Biavati G, Bidlot J, Bonavita M, De Chiara G, Dahlgren P, Dee D, Diamantakis M, Dragani R, Flemming J, Forbes R, Fuentes M, Geer A, Haimberger L, Healy S, Hogan RJ, Hólm E, Janisková M, Keeley S, Laloyaux P, Lopez P, Lupu C, Radnoti G, de Rosnay P, Rozum I, Vamborg F, Villaume S, Thépaut JN (2020) The ERA5 global reanalysis. Q J R Meteor Soc 146(730):1999–2049. https://doi.org/10.1002/qj.3803

Huete AR (1988) A soil-adjusted vegetation index (SAVI). Remote Sens Environ 25(3):295–309. https://doi.org/10.1016/0034-4257(88)90106-X

Italiano SSP, Camarero JJ, Borghetti M, Colangelo M, Rita A, Ripullone F (2024) Drought legacies in mixed Mediterranean forests: analysing the effects of structural overshoot, functional traits and site factors. Sci Total Environ 927:172166. https://doi.org/10.1016/j.scitotenv.2024.172166

Jacovides CP, Tymvios FS, Asimakopoulos DN, Theofilou KM, Pashiardes S (2003) Global photosynthetically active radiation and its relationship with global solar radiation in the Eastern Mediterranean basin. Theor Appl Climatol 74(3):227–233. https://doi.org/10.1007/s00704-002-0685-5

Keeley JE (2009) Fire intensity, fire severity and burn severity: a brief review and suggested usage. Int J Wildland Fire 18(1):116–126. https://doi.org/10.1071/wf07049

Kolb TE, Stone JE (2000) Differences in leaf gas exchange and water relations among species and tree sizes in an Arizona pine-oak forest. Tree Physiol 20(1):1–12. https://doi.org/10.1093/treephys/20.1.1

Körner C, Sarris D, Christodoulakis D (2005) Long-term increase in climatic dryness in the East-Mediterranean as evidenced for the island of Samos. Reg Environ Change 5(1):27–36. https://doi.org/10.1007/s10113-004-0091-x

Marx A, Kleinschmit B (2017) Sensitivity analysis of RapidEye spectral bands and derived vegetation indices for insect defoliation detection in pure Scots pine stands. Iforest 10(4):659–668. https://doi.org/10.3832/ifor1727-010

Mazza G, Markou L, Sarris D (2021) Species-specific growth dynamics and vulnerability to drought at the single tree level in a Mediterranean reforestation. Trees 35(5):1697–1710. https://doi.org/10.1007/s00468-021-02151-6

Mazza G, Sarris D (2021) Identifying the full spectrum of climatic signals controlling a tree species' growth and adaptation to climate change. Ecol Indic 130:108109. https://doi.org/10.1016/j.ecolind.2021.108109

Mazza G, Sarris D, Chiavetta U, Ferrara RM, Rana G (2018) An intra-stand approach to identify intra-annual growth responses to climate in *Pinus nigra* subsp. *laricio* Poiret trees from southern Italy. For Ecol Manage 425:9–20. https://doi.org/10.1016/j.foreco.2018.05.029

McMahon SM, Arellano G, Davies SJ (2019) The importance and challenges of detecting changes in forest mortality rates. Ecosphere 10(2):e02615. https://doi.org/10.1002/ecs2.2615

Meteorological Service (1986) The climate of Cyprus

Moreno-de-las-Heras M, Bochet E, Vicente-Serrano SM, Espigares T, Molina MJ, Monleón V, Nicolau JM, Tormo J, García-Fayos P (2023) Drought conditions, aridity and forest structure control the responses of Iberian holm oak woodlands to extreme droughts: a large-scale remote-sensing exploration in eastern Spain. Sci Total Environ 901:165887. https://doi.org/10.1016/j.scitotenv.2023.165887

Moritz S, Bartz-Beielstein T (2017) imputeTS: time series missing value imputation in R. R J 9(1):207. https://doi.org/10.32614/rj-2017-009

National Centers for Environmental Information (NCEI) (2025) Daily observational data.

Pashiardis S, Michaelides SC (2009) Implementation of the standardized precipitation index (SPI) and the reconnaissance drought index (RDI) for regional drought assessment: a case study for Cyprus.

Peguero-Pina JJ, Sancho-Knapik D, Ferrio JP, López-Ballesteros A, Ruiz-Llata M, Gil-Pelegrín E (2023) Reevaluating near-infrared reflectance as a tool for the study of plant water status in holm oak (*Quercus ilex* subsp. *rotundifolia*). Forests 14(9):1825. https://doi.org/10.3390/f14091825

Reyer CPO, Leuzinger S, Rammig A, Wolf A, Bartholomeus RP, Bonfante A, de Lorenzi F, Dury M, Gloning P, Abou Jaoudé R, Klein T, Kuster TM, Martins M, Niedrist G, Riccardi M, Wohlfahrt G, de Angelis P, de Dato G, François L, Menzel A, Pereira M (2013)

A plant's perspective of extremes: terrestrial plant responses to changing climatic variability. Glob Change Biol 19(1):75–89. https://doi.org/10.1111/gcb.12023

Rouse JW Jr (1974) Monitoring vegetation systems in the great plains with erts. In: NASA Special Publication. NASA, p 309

Sarris D, Christodoulakis D (2024) Topographic and climatic effects on *Pinus halepensis* s.l. growth at its drought tolerance margins under climatic change. J for Res 35(1):102. https://doi.org/10.1007/s11676-024-01755-1

Sarris D, Christodoulakis D, Körner C (2011) Impact of recent climatic change on growth of low elevation eastern Mediterranean forest trees. Clim Change 106(2):203–223. https://doi.org/10.1007/s10584-010-9901-y

Sarris D, Christodoulakis D, Körner C (2007) Recent decline in precipitation and tree growth in the eastern Mediterranean. Glob Change Biol 13(6):1187–1200. https://doi.org/10.1111/j.1365-2486.2007.01348.x

Sarris D, Mazza G (2021a) Pines and their mixed forest ecosystems in the Mediterranean Basin. In: Osem Y (ed) Ne'eman G. Pines and their mixed forest ecosystems in the Mediterranean Basin. Springer International Publishing, Cham, pp 129–140

Sarris D, Mazza G (2021) Mediterranean pine root systems under drought. In: Pines and their mixed forest ecosystems in the Mediterranean Basin. Springer International Publishing, pp 129–140. https://doi.org/10.1007/978-3-030-63625-8_8

Sarris D, Siegwolf R, Körner C (2013) Inter- and intra-annual stable carbon and oxygen isotope signals in response to drought in Mediterranean pines. Agric for Meteor 168:59–68. https://doi.org/10.1016/j.agrformet.2012.08.007

Seager R, Ting MF, Held I, Kushnir Y, Lu J, Vecchi G, Huang HP, Harnik N, Leetmaa A, Lau NC, Li CH, Velez J, Naik N (2007) Model projections of an imminent transition to a more arid climate in southwestern North America. Science 316(5828):1181–1184

Sellers PJ, Berry JA, Collatz GJ, Field CB, Hall FG (1992) Canopy reflectance, photosynthesis, and transpiration. III. A reanalysis using improved leaf models and a new canopy integration scheme. Remote Sens Environ 42(3):187–216. https://doi.org/10.1016/0034-4257(92)90102-P

Sheil D (2018) Forests, atmospheric water and an uncertain future: the new biology of the global water cycle. For Ecosyst 5:19. https://doi.org/10.1186/s40663-018-0138-y

Shukla S, Safeeq M, AghaKouchak A, Guan KY, Funk C (2015) Temperature impacts on the water year 2014 drought in California. Geophys Res Lett 42(11):4384–4393. https://doi.org/10.1002/2015GL063666

Stefanidis S, Rossiou D, Proutsos N (2023) Drought severity and trends in a Mediterranean oak forest. Hydrology 10(8):167. https://doi.org/10.3390/hydrology10080167

Stephenson NL, van Mantgem PJ, Bunn AG, Bruner H, Harmon ME, O'Connell KB, Urban DL, Franklin JF (2011) Causes and implications of the correlation between forest productivity and tree mortality rates. Ecol Monogr 81(4):527–555. https://doi.org/10.1890/10-1077.1

Thom D, Seidl R, Steyrer G, Krehan H, Formayer H (2013) Slow and fast drivers of the natural disturbance regime in Central European forest ecosystems. For Ecol Manag 307:293–302. https://doi.org/10.1016/j.foreco.2013.07.017

Tomppo E, Gschwantner T, Lawrence M, McRoberts RE (2010) National forest inventories: pathways for common reporting. Springer Netherlands. https://doi.org/10.1007/978-90-481-3233-1

Townsend PA, Singh A, Foster JR, Rehberg NJ, Kingdon CC, Eshleman KN, Seagle SW (2012) A general Landsat model to predict canopy defoliation in broadleaf deciduous forests. Remote Sens Environ 119:255–265. https://doi.org/10.1016/j.rse.2011.12.023

USGS (2025) Landsat Enhanced Vegetation Index. In: USGS. https://www.usgs.gov/landsat-missions/landsat-enhanced-vegetation-index. Accessed 20 Aug 2025

van Mantgem PJ, Stephenson NL, Byrne JC, Daniels LD, Franklin JF, Fulé PZ, Harmon ME, Larson AJ, Smith JM, Taylor AH, Veblen TT (2009) Widespread increase of tree mortality rates in the western United States. Science 323(5913):521–524. https://doi.org/10.1126/science.1165000

Verbesselt J, Hyndman R, Zeileis A, Culvenor D (2010) Phenological change detection while accounting for abrupt and gradual trends in satellite image time series. Remote Sens Environ 114(12):2970–2980. https://doi.org/10.1016/j.rse.2010.08.003

Vetter M, Churkina G, Jung M, Reichstein M, Zaehle S, Bondeau A, Chen Y, Ciais P, Feser F, Freibauer A, Geyer R, Jones C, Papale D, Tenhunen J, Tomelleri E, Trusilova K, Viovy N, Heimann M (2008) Analyzing the causes and spatial pattern of the European 2003 carbon flux anomaly using seven models. Biogeosciences 5(2):561–583. https://doi.org/10.5194/bg-5-561-2008

Vicente-Serrano SM, Beguería S, López-Moreno JI (2010) A multiscalar drought index sensitive to global warming: the standardized precipitation evapotranspiration index. J Clim 23(7):1696–1718. https://doi.org/10.1175/2009jcli2909.1

Wu CY, Niu Z, Gao S (2010) Gross primary production estimation from MODIS data with vegetation index and photosynthetically active radiation in maize. J Geophys Res Atmos 115(D12):2009JD013023. https://doi.org/10.1029/2009JD013023

Xue JR, Su BF (2017) Significant remote sensing vegetation indices: a review of developments and applications. J Sens 2017(1):1353691. https://doi.org/10.1155/2017/1353691

Zhang YL, Moser B, Li MH, Wohlgemuth T, Lei JP, Bachofen C (2020) Contrasting leaf trait responses of conifer and broadleaved seedlings to altered resource availability are linked to resource strategies. Plants 9(5):621. https://doi.org/10.3390/plants9050621